Fractal dragon curve microstrip antenna for Dual-Band WLAN communications

Karol Dragowski, Mateusz Pasternak

Abstract—The growing usage of wireless networks and the reduction of device sizes requires the search for new solutions in antenna technology. This study presents a direct-fed microstrip antenna, which is based on the Dragon Curve fractal and operates at two resonances: 2.4 and 5 GHz, frequencies commonly used in wireless communications. The antenna dimensions are 4.25 by 2.84 cm. The simulated reflection coefficients for the resonances are -36.49 and -30.73 dB, while the measured values are -14.68 and -14.85 dB.

Keywords—fractal antenna, microstrip antenna, WLAN antenna, dual-band antenna, dragon curve

I. INTRODUCTION

THE widely used wireless local area network (WLAN) communication standard is IEEE 802.11. Wi-Fi is used by many internet users and IoT (Internet of Things) devices. It is estimated that in 2023 was approximately 5.3 billion total Internet users and 628 million public Wi-Fi hotspots [1]. Numerous transmitting and receiving devices require different antenna systems, including those with two bands – 2.4 and 5 GHz. Fractals make the shape practical for operation at two resonant frequencies, while still keeping it small. Additionally, the use of microstrip technology has reduced manufacturing costs.

A fractal typically describes an object that is self-similar, meaning its parts resemble the whole. It may also denote an infinitely intricate object displaying progressively complex details at infinitely high magnification. Benoit Mandelbrot published a paper [2] in 1967 that connected the concepts of mathematicians to real-world phenomena, specifically self-similar coastlines. He established that self-similarity methods can be a useful tool in analyzing random occurrences across multiple fields, such as geostatistics, economics, and physics. Consequently, fractals have been adopted in several scientific disciplines.

One method for creating fractals is the Iterated Function System (IFS). It is a family of functions that are affine transformations. The vector w defines such operations as follows:

$$w \begin{bmatrix} x \\ y \end{bmatrix} = \begin{bmatrix} a & b \\ c & d \end{bmatrix} \begin{bmatrix} x \\ y \end{bmatrix} + \begin{bmatrix} e \\ f \end{bmatrix} \tag{1}$$

K. Dragowski is with Unmanned Systems and Balistics Centre, Military Institute of Armament Technology, Zielonka, Poland (e-mail: dragowskik@witu.mil.pl).

M. Pasternak is with Institute of Radioelectronics, Military University of Technology, Warsaw, Poland (e-mail: mateusz.pasternak@wat.edu.pl).

where a, b, c and d coefficients represent figure rotation and scaling, while e and f represent linear translation. If a series of transformations are applied: $w_1, w_2, \ldots, w_N$, on the figure A, which is the base figure, one gets the figure described as:

$$W(A) = U_{n=1}^N w_n(A), \tag{2}$$

where W is called the Hutchinson operator. The fractal figure will be created after several times, applying the operator W to the initial figure.

Fractals have found applications in many fields of science. Image compression, capacitor design, fluid mechanics or fracture mechanics and plant classification are among the many examples of fractal applications. Antennas with fractal shaped radials started to appear from 1993 [3]. The potential in the use of fractal shapes was noted by N. Cohen [4], [5]. Then other fractals began to be widely used in antenna technology. Koch curve [6], [7], Sierpinski carpet [8], [9], Sierpinski triangle [10], [11], Hilbert curve [12], [13] and Cantor set [14], Minkowski fractal [15] and Mandelbrot set [16] were used for antenna design.

The dragon curve was used in [17], coplanar feeding was applied and 6 consecutive iterations of this fractal were examined. The dimensions of each section (L) were scaled by $L/\sqrt{2}$. One or two resonances between 3 and 8.4 GHz were achieved. A modified fractal of the 8th iteration has been used in [18] for application of an ultra-wideband RFID (Radio Frequency Identification) tag. The [19]–[21] used modified dragon curves in combination with other fractals.

The paper outlines how the dragon curve can be applied to microstrip technology for dual band Wi-Fi applications. Despite its potential, this fractal has yet to see much practical use without deep modifications.

II. ANTENNA CONSTRUCTION

A. Dragon curve fractal

The Dragon curve (also known as the Harter-Heighway curve) was invented by physicists John Heighway, Bruce Banks and William Harter, and described in Recreational Mathematics [22] by C. Davis and D. Knuth. The starting figure for the construction of this fractal is the segment. Subsequent iterations involve scaling by $r = 1/\sqrt{2}$ the figure from the previous step and placing it so that the original segment is the isosceles triangle's counter-rectangle formed by the two segments after scaling. The fractal dimension is
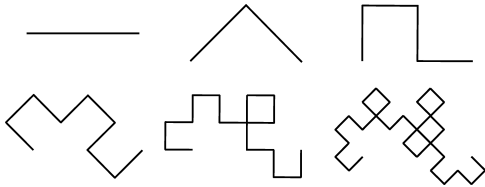
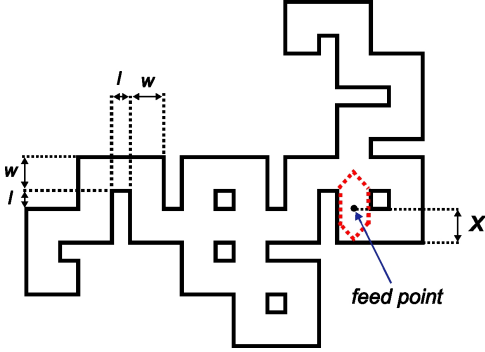Fig. 1. First five iterations of the fractal

Fig. 2. Proposed antenna based on dragon curve 5th iteration

approximately 1.524. Figure 1 shows the first five iterations. The description using the IFS takes the following form:

$$f_1(x) = \begin{bmatrix} \frac{1}{2} & -\frac{1}{2} \\ \frac{1}{2} & \frac{1}{2} \end{bmatrix} x, \tag{3}$$

$$f_2(x) = \begin{bmatrix} -\frac{1}{2} & -\frac{1}{2} \\ \frac{1}{2} & -\frac{1}{2} \end{bmatrix} x + \begin{bmatrix} 1 \\ 0 \end{bmatrix}, \tag{4}$$

Dragon curve can also be set up as non-self-crossing space-filling curve with a fractal dimension of 2.

B. Antenna construction

The proposed antenna is based on a dragon curve fractal of the 5th iteration. The fractal sections were implemented as microstrip rectangular patches of width (w) and length (l) and connected to each other by squares of length (w). Antenna feeding is realized through a direct probe in the centre of the width of segment ($x/2$) and its position is relative to the axis along the segment (x). Iteration and segment were chosen arbitrarily, based on previous research by the authors. The values of these parameters were chosen by simulation to obtain the best matching in the operating bands of the Wi-Fi network. The simulations were carried out using CST Microwave Studio software. Time Domain Solver was used. Figure 2 shows the shape of the antenna. The red dashed line indicates the area where the feed point was searched. The construction uses FR4 substrate with a permittivity ε of 4.6 and a thickness of 1.5 mm with a 0.035 mm thick copper layer. The area of the substrate, which is a rectangle rotated by $45°$, is designed so that each edge is at a distance w from the radiating surface. In order to find the best match between the antenna and the feed line (with impedance equal 50 Ω), an optimization of the x, w and l parameters was performed. Three parameters were considered in the search for the best return loss. Segment dimensions (length and width) and feed position (l, w, x respectively).
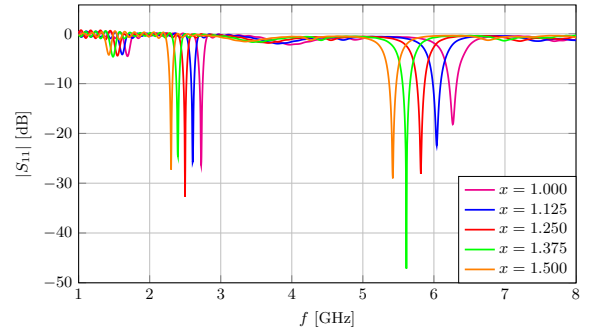

Fig. 3. Return loss ($|S_{11}|$) depending on changing x value

In order to obtain the correct resonance pattern, the starting point was determined based on previous research. Changing the feed position while keeping the dimensions constant will affect the value of $|S_{11}|$ in each resonance. To describe this value, the variable γ was introduced.

$$\gamma = \frac{x}{l + w} \tag{5}$$

Changing the length and width of a segment affects the resonance placement. This was hard to achieve, so the work was divided into parts. The first step was to establish the feed point. The value of γ was considered between 0 and 1. The

TABLE I
SUMMARY OF REFLECTION COEFFICIENT RESULTS IN RELATION TO CHANGE IN γ VALUE

γ	f_1 [GHz]	f_2 [GHz]	$|S_{11}|$ of f_1 [dB]	$|S_{11}|$ of f_2 [dB]
0	2.30	5.54	-24.27	-12.48
0.125	2.30	5.51	-22.90	-13.15
0.250	2.30	5.47	-23.06	-15.58
0.375	2.30	5.42	-27.26	-28.70
0.500	2.30	5.37	-22.20	-13.75
0.625	2.29	5.34	-22.40	-6.59
0.750	2.29	5.32	-21.70	> -5
0.875	2.28	—	-16.53	—
1.000	2.28	—	-13.93	—

best value of γ was 0.375 and this was used for the next steps in the antenna design. In the next step, the return loss ($|S_{11}|$) was taken into account for a change in the value of x with the other considered parameters fixed. The effect of changing this parameter is shown in Fig. 3. The resonant frequencies can be determined from equations that are based on these characteristics:

$$f_1(x) = -0.834x + 3.541 \tag{6}$$

$$f_2(x) = -1.686x + 7.931 \tag{7}$$

The value 1.31 was chosen for x. In the next step the same method was used to find the value of w (with fixed x and γ) and the results are shown in Fig. 4. Similarly, the equations for the resonant frequency depending on the segment width were determined, which have the form:

$$f_1(w) = -0.7w + 4.195 \tag{8}$$

$$f_2(w) = -1.652w + 9.848 \tag{9}$$

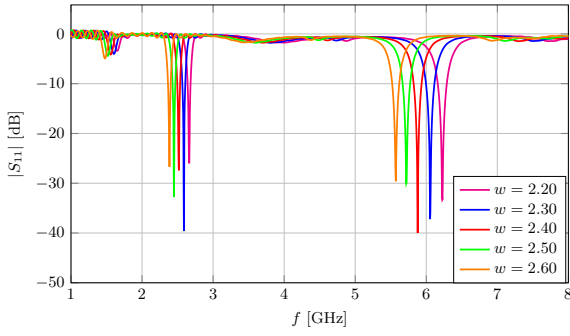Fig. 4. Return loss ($|S_{11}|$) depending on changing w value

The value 2.45 of w has been chosen. The final step is to optimize γ for the best value of the return loss. The value 0.338 of γ was chosen. The result is an antenna measuring 42.52 by 28.41 mm. Table II summarizes all antenna dimensions. An-

TABLE II
SUMMARY OF ANTENNA DIMENSIONS.

Parameter name	Parameter symbol	Value
Length of section	l	1.31 mm
Width of section	w	2.45 mm
Feed point position	x	1.27 mm
Antenna length	L	42.52 mm
Antenna width	W	28.41 mm

tenna was manufactured and measured with Keysight N9952A Microwave Analyzer. Figure 5 shows proposed antenna.
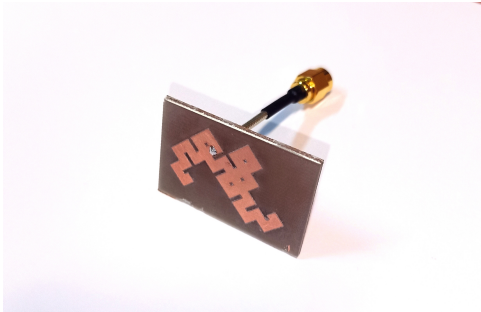

Fig. 5. Manufactured antenna

III. RESULTS

A. Reflection coefficient

For determining the bandwidth, a standard level of -10 dB of return loss was assumed. This means that 90% of energy is transmitted through antenna and 10% reflected. In the proposed antenna there are two narrow bands. Figure 6 shows the reflection coefficient as a function of frequency, comparing simulated and measured results. In simulations the following results were obtained. First resonance at 2.464 — 2.504 GHz (with a width of 40 MHz) and second resonance at 5.760 — 5.874 GHz (114 MHz). The values of the coefficient $|S_{11}|$ are equal to -36.49 and -30.73 dB, respectively. In these resonances, the antenna can be used for WLAN 2,4/5 GHz
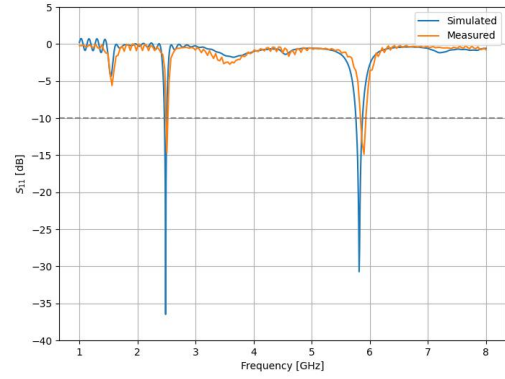

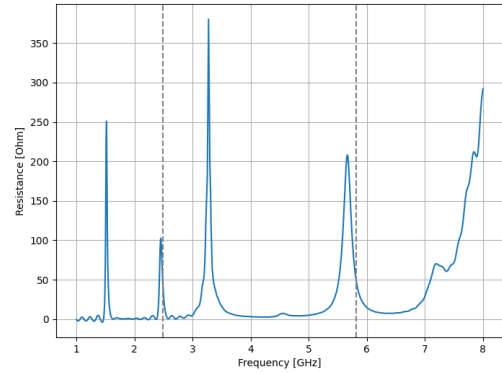Fig. 6. The reflection coefficient as a function of frequency.

Fig. 7. Real part of impedance depend on frequency.

communication (WiFi, 2.4 GHz, 802.11b/g/n/ax IEEE standard and 5 GHz 802.11a/h/n/ac/ax IEEE standard [1]). The measured antenna has resonances at 2.47 and 5.90 GHz with coefficient $|S_{11}|$ equal to - 14.68 and - 14.85 dB respectively, which is very good accuracy of the simulations. A fairly narrow band is achieved, which is desirable in communications applications.

B. Input impedance

The antenna is designed for 50 Ω feedline. For assumed bandwidth it is expected that real part of impedance and imaginary part (value close to 0) will match. On figure 7 is shown real part of impedance according to frequency, dotted grey line shows resonance frequencies which value for this point is 50.06 and 49.36 Ω respectively. The imaginary part of the frequency dependent impedance is shown in figure 8. The values of reactance for this resonance are 1.50 and -2.82 Ω respectively.

C. Radiation characteristics

Radiation patterns show the distribution of energy in three dimensions. Figures 9 and 10 show the antenna radiation pattern in relation to an isotropic antenna. Figure 11 shows the
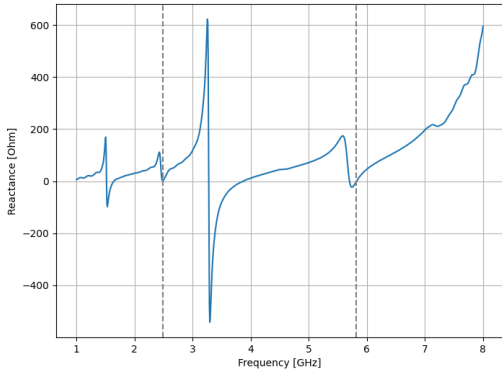
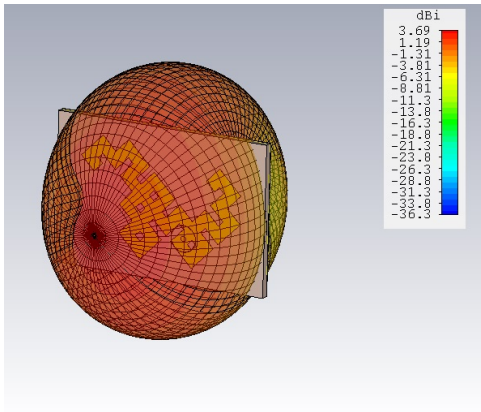Fig. 8. Imaginary part of impedance depend on frequency.

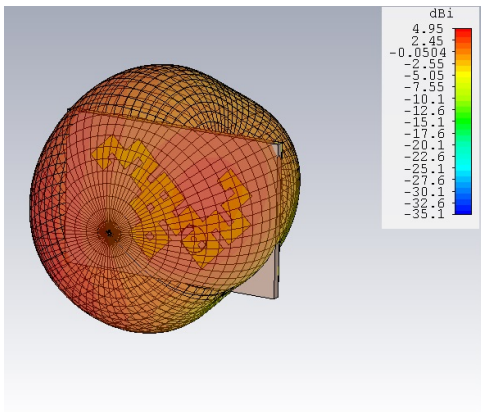Fig. 9. The 3D radiation pattern for $f = 2.484$ GHz.

Fig. 10. The 3D radiation pattern for $f = 5.816$ GHz.

Fig. 11. Normalized radiation pattern at resonant $f = 2.484$ GHz.
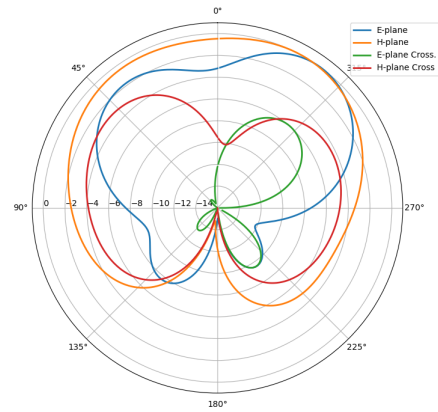
Fig. 12. Normalized radiation pattern at resonant $f = 5.816$ GHz.

normalized radiation pattern for the first resonance. There is a slight shift of the characteristic E-plane maximum with respect to the front of the antenna and a back lobe is present due to the limited ground plane. The maximum gain is 3.69 dBi. The cross-polarization pattern is separated by 4 dB. The H-plane also has a back lobe and the maximum gain is 3.55 dBi. The cross-polarization pattern is also separated by 4 dB. The normalized radiation pattern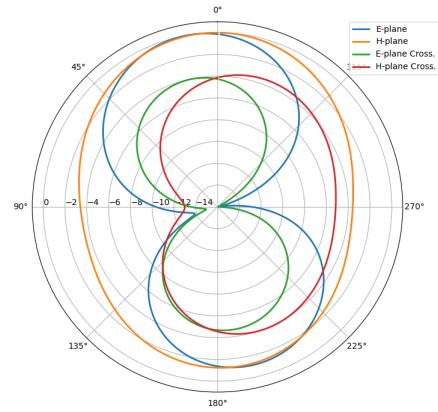 for the second resonance is shown in figure 12, where the E-plane has a cardioid radiation pattern with a maximum at 4.95 dBi. The cross-polarization pattern is 6 dB lower. For the H-plane the maximum is 2.2 dBi and the cross-polarization discrimination is about 3 dB. For this resonance, the back radiation is attenuated according to the first, but still exists.

D. Current distribution

Figures 13 and 14 show the current distribution across the antenna aperture for each resonant frequency. At each resonance, a different current density can be observed at a different location. The rather complicated shape of the antenna implies a different distribution of currents at different operating frequencies, which is the reason for the multiband nature of the antennas. The direct feed, which was used in the proposed antenna, has a much impact effect on radiation than a microstrip feed, which also radiates and affects the radiation characteristics.

TABLE III
PERFORMANCE COMPARISON BETWEEN THE PROPOSED ANTENNA WITH THE EXISTING REPORTED ANTENNAS.

| Reference No.	Dimensions (λ_L)	Resonant frequencies [GHz]	Bandwidth	Gain [dBi]	f_h/f_l
[23]	0.15×0.44	0.73, 3.53	17.93%, 14.16%	2.40, 6.10	4,9
[24]	0.21×0.09	0.91, 2.45	1.97%, 0.55%	2.87, 6.80	2,7
[25]	0.41×0.60	2.40, 5.80	12.92%, 9.83%	N/A	2,4
[26]	0.65×0.60	8.80, 11.30	2.00%, 1.40%	5.30, 4.30	1,3
[27]	0.31×0.31	2.40, 2.80	N/A	3.42, 3.20	1,2
[28]	0.60×0.60	2.40, 5.50	13.00%, 27.00%	6.80, 9.00	2,3
[29]	0.60×0.60	1.90, 3.50	4.00%, 2.20%	1.00, 2.40	1,8
[30]	0.60×0.60	2.40, 5.40	3.96%, 0.93%	2.87, 6.80	2,3
Proposed work	0.24×0.38	2.48, 5.82	1.61%, 1.96%	3.69, 4.95	2,3
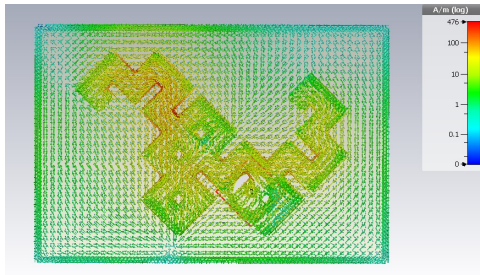
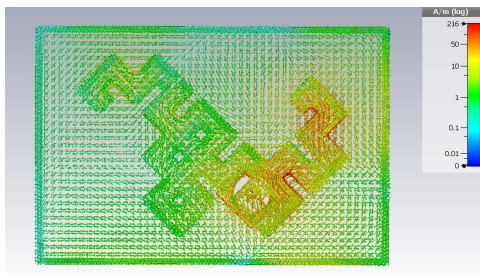Fig. 13. Current distribution for $f = 2.484$ GHz.

Fig. 14. Current distribution for $f = 5.816$ GHz.

E. Performance comparison

The performance comparison with other research on dual band antennas is presented in Table III. The proposed antenna has small dimensions in relation to the wavelength[1] of the lower resonance frequency, but also has a very narrow bandwidth.

IV. CONCLUSIONS

This article presents a dual-band microstrip antenna designed for WLAN applications using the fifth iteration of the dragon curve fractal. A small size of 42.52 x 28.41 mm has been achieved. The antenna resonates at 2.4 and 5 GHz with a simulated reflection coefficient of less than -30 dB. The proposed antenna has a directivity at resonances of more than 3.69 and 4.95 dBi. Its suitability for use in communication systems utilizing both WiFi frequencies (2.4 and 5 GHz) is

---

[1]wavelength at the lowest resonant frequency

demonstrated. Manufactured antenna has reflection coefficient of less than -14 dB with a resonances near to simulated.

REFERENCES

[1] "Ieee standard for information technology—telecommunications and information exchange between systems local and metropolitan area networks—specific requirements - part 11: Wireless lan medium access control (mac) and physical layer (phy) specifications," *IEEE Std 802.11-2016 (Revision of IEEE Std 802.11-2012)*, pp. 1–3534, 2016. [Online]. Available: https://doi.org/10.1109/IEEESTD.2016.7786995

[2] B. Mandelbrot, "How long is the coast of britain? statistical self-similarity and fractional dimension," *science*, vol. 156, no. 3775, pp. 636–638, 1967. [Online]. Available: https://doi.org/10.1126/science.156.3775.636

[3] D. Werner, "Fractal radiators," in *Proceedings of the 4th Annual 1994 IEEE Mohawk Valley Section Dual-Use Technologies & Applications Conference*, vol. 1, pp. 23–26.

[4] N. Cohen, "Fractal antennas," vol. 9, p. 1995.

[5] N. Cohen and R. Hohlfeld, "Fractal loops and the small loop approximation," vol. 6, no. 2, pp. 77–81.

[6] C. Puente, J. Romeu, R. Pous, J. Ramis, and A. Hijazo, "Small but long koch fractal monopole," vol. 34, no. 1, pp. 9–10. [Online]. Available: https://doi.org/10.1049/el:19980114

[7] C. P. Baliarda, J. Romeu, and A. Cardama, "The koch monopole: A small fractal antenna," vol. 48, no. 11, pp. 1773–1781. [Online]. Available: https://doi.org/10.1109/8.900236

[8] C. Puente Baliarda, J. Romeu Robert, R. Pous Andrés, X. Garcia, and F. Benitez, "Fractal multiband antenna based on the sierpinski gasket," *Electronics Letters*, vol. 32, no. 1, pp. 1–2, 1996. [Online]. Available: https://doi.org/10.1049/el:19960033

[9] J. S. Sivia, G. Kaur, and A. K. Sarao, "A modified sierpinski carpet fractal antenna for multiband applications," *Wireless Personal Communications*, vol. 95, pp. 4269–4279, 2017. [Online]. Available: https://doi.org/10.1007/s11277-017-4079-5

[10] C. Puente-Baliarda, J. Romeu, R. Pous, and A. Cardama, "On the behavior of the sierpinski multiband fractal antenna," vol. 46, no. 4, pp. 517–524. [Online]. Available: https://doi.org/10.1109/8.664115

[11] P. S. R. Chowdary, A. M. Prasad, P. M. Rao, and J. Anguera, "Design and performance study of sierpinski fractal based patch antennas for multiband and miniaturization characteristics," *Wireless Personal Communications*, vol. 83, pp. 1713–1730, 2015. [Online]. Available: https://doi.org/10.1007/s11277-015-2472-5

[12] K. Vinoy, K. Jose, V. Varadan, and V. Varadan, "Hilbert curve fractal antenna: A small resonant antenna for VHF/UHF applications," vol. 29, no. 4, pp. 215–219. [Online]. Available: https://doi.org/10.1002/mop.1136

[13] D.-C. Chang, B.-H. Zeng, J.-C. Liu, I. Chen, L.-G. Jang, and C.-C. Chang, "A self-complementary hilbert-curve fractal antenna for UHF RFID tag applications," in *2008 IEEE Antennas and Propagation Society International Symposium*. IEEE, pp. 1–4. [Online]. Available: https://doi.org/10.1109/APS.2008.4619585

[14] I. Masroor, J. Ansari, and A. K. Saroj, "Inset-fed cantor set fractal multiband antenna design for wireless applications," in *2020 International Conference for Emerging Technology (INCET)*. IEEE, 2020, pp. 1–4. [Online]. Available: https://doi.org/10.1109/INCET49848.2020.9154012

[15] M. Comisso, "Theoretical and numerical analysis of the resonant behaviour of the minkowski fractal dipole antenna," *IET microwaves, antennas & propagation*, vol. 3, no. 3, pp. 456–464, 2009. [Online]. Available: https://doi.org/10.1049/iet-map.2008.0249

[16] J. Anguera, A. Andújar, S. Benavente, J. Jayasinghe, and S. Kahng, "High-directivity microstrip antenna with mandelbrot fractal boundary," *IET Microwaves, Antennas & Propagation*, vol. 12, no. 4, pp. 569–575, 2018. [Online]. Available: https://doi.org/10.1049/iet-map.2017.0649

[17] A. Reha, A. Elamri, and O. Benhmammouch, *CPW-Fed Dragon Fractal Antenna for UWB Applications*, 11 2017, vol. 397, pp. 423–429. [Online]. Available: https://doi.org/10.1007/978-981-10-1627-1_33

[18] T. Abo-Elnaga, E. Abdallah, and H. El-Hennawy, "Novel dragon shape uhf rfid tag antenna," *a a*, vol. 2, no. 1, p. 2. [Online]. Available: https://www.academia.edu/23644157/Novel_Dragon_Shape_UHF_RFID_Tag_Antenna

[19] S. Rajkumar, N. Srinivasan, A. Natesan, and K. T. Selvan, "A penta-band hybrid fractal mimo antenna for ism applications," *International Journal of RF and Microwave Computer-Aided Engineering*, vol. 28, no. 2, p. e21185, 2018. [Online]. Available: https://doi.org/10.1002/mmce.21185

[20] D. H. Werner, W. Kuhirun, and P. L. Werner, "Fractile arrays: A new class of tiled arrays with fractal boundaries," *IEEE Transactions on Antennas and Propagation*, vol. 52, no. 8, pp. 2008–2018, 2004. [Online]. Available: https://doi.org/10.1109/TAP.2004.832327

[21] N. Sharma and S. S. Bhatia, "Comparative analysis of hybrid fractal antennas: A review," *International Journal of RF and Microwave Computer-Aided Engineering*, vol. 31, no. 9, p. e22762, 2021. [Online]. Available: https://doi.org/10.1002/mmce.22762

[22] C. Davis and D. E. Knuth, "Number representations and dragon curves," vol. 3, no. 2, pp. 66–81.

[23] A. K. Arya, S. J. Kim, and S. Kim, "A dual-band antenna for lte-r and 5g lower frequency operations," *Progress In Electromagnetics Research Letters*, vol. 88, pp. 113–119, 2020. [Online]. Available: https://doi.org/10.2528/PIERL19081502

[24] M. Najumunnisa, A. S. C. Sastry, B. T. P. Madhav, S. Das, N. Hussain, S. S. Ali, and M. Aslam, "A metamaterial inspired amc backed dual band antenna for ism and rfid applications," *Sensors*, vol. 22, no. 20, p. 8065, 2022. [Online]. Available: https://doi.org/10.3390/s22208065

[25] P. B. Nayak, R. Endluri, S. Verma, and P. Kumar, "A novel compact dual-band antenna design for wlan applications," *arXiv preprint arXiv:2106.13232*, 2021. [Online]. Available: https://doi.org/10.48550/arXiv.2106.13232

[26] A. A. Althuwayb, M. J. Al-Hasan, A. Kumar, and D. Chaturvedi, "Design of half-mode substrate integrated cavity inspired dual-band antenna," *International Journal of RF and Microwave Computer-Aided Engineering*, vol. 31, no. 2, p. e22520, 2021. [Online]. Available: https://doi.org/10.1002/mmce.22520

[27] W. M. Abdulkawi, A. F. A. Sheta, I. Elshafiey, and M. A. Alkanhal, "Design of low-profile single-and dual-band antennas for iot applications," *Electronics*, vol. 10, no. 22, p. 2766, 2021. [Online]. Available: https://doi.org/10.3390/electronics10222766

[28] C. Shi, J. Zou, J. Gao, and C. Liu, "Gain enhancement of a dual-band antenna with the fss," *Electronics*, vol. 11, no. 18, p. 2882, 2022. [Online]. Available: https://doi.org/10.3390/electronics11182882

[29] A. Jafargholi, A. Jafargholi, and B. Ghalamkari, "Dual-band slim microstrip patch antennas," *IEEE Transactions on Antennas and Propagation*, vol. 66, no. 12, pp. 6818–6825, 2018. [Online]. Available: https://doi.org/10.1109/TAP.2018.2871964

[30] A. Wajid, A. Ahmad, S. Ullah, D.-y. Choi, and F. U. Islam, "Performance analysis of wearable dual-band patch antenna based on ebg and srr surfaces," *Sensors*, vol. 22, no. 14, p. 5208, 2022. [Online]. Available: https://doi.org/10.3390/s22145208